Perpendicular magnetic anisotropy of epitaxially grown $L1_0$-FePdCu nanoparticles with preferential *c*-axis orientation

Hiroshi Naganuma,[a] Kazuhisa Sato, and Yoshihiko Hirotsu
The Institute of Scientific and Industrial Research, Osaka University, 8-1 Mihogaoka, Ibaraki, Osaka 567-0047, Japan

(Received 31 March 2006; accepted 21 July 2006; published online 13 October 2006)

Oriented and well-isolated 14-nm-sized $Fe_{41}Pd_{52}Cu_7$ ternary alloy nanoparticles with the $L1_0$-type ordered structure have been fabricated by the sequential deposition of Pd, Cu, and Fe on NaCl (001) substrate followed by postdeposition annealing. The annealing temperature required to obtain a high coercivity decreased by at least 50 K upon the addition of a small amount of Cu. Furthermore, it was revealed that a strong preferential *c*-axis orientation along the film normal direction was achieved by the addition of Cu, which resulted in a strong perpendicular magnetic anisotropy. The population of the nanoparticles with their *c*-axis oriented normal to the film plane was 74%. The alloy composition was independent of the particle size, as determined by energy dispersive x-ray spectroscopy using nanoprobe electrons. Nanobeam electron diffraction revealed that the axial ratio is constant for FePdCu nanoparticles with sizes between 10 and 25 nm. Interparticle magnetostatic and exchange interactions played an insignificant role in the isolated FePdCu nanoparticles. The correlation between their preferential *c*-axis orientation and magnetic properties is discussed based on the rotation magnetization of single magnetic domain particles. © *2006 American Institute of Physics*. [DOI: 10.1063/1.2357420]

I. INTRODUCTION

Magnetic recording has been used as a leading method for high-density data storage. In the near future, the areal density of magnetic recording media will become as high as 1 Tbit/in.^{2} (Refs. 1 and 2). For such a high recording density, the magnetic memory size will become several tens of nanometers in diameter with edge-to-edge distances of a few nanometers. In these nanosized scale magnetic media, the recording noise due to the thermal fluctuation of magnetic moments limits the recording density. One of the candidate materials suitable for ultrahigh-density magnetic recording with less noise is an assembly of isolated, hard magnetic nanoparticles with high magnetic anisotropy energy together with an aligned magnetic easy axis. In this regard, $L1_0$-type FePt, FePd, and CoPt ordered alloys have attracted considerable attention because of their large uniaxial magnetic anisotropy energy,[3] which ensures the thermal stability of magnetic moments in nanometer-sized particles. The magnetization process of fine isolated nanoparticles is characterized by rotation magnetization against the anisotropy energy barrier, which has been established by theoretical and experimental studies written about in several review articles.[4,5] Recently, many studies have focused on the fabrication of $L1_0$-FePt, FePd, and CoPt nanoparticles with high coercivities.[6] However, a high-temperature heat treatment such as substrate heating during deposition and/or postdeposition annealing at temperatures around 873 K is usually necessary for the formation of the $L1_0$-ordered phase in isolated nanoparticles produced by physical evaporation or chemical synthesis, since a metastable disordered phase is usually formed in the as-deposited specimens.[7,8] Such high-temperature annealing is not suitable for industrial applications; hence, an effective method for decreasing the ordering temperature is required.

The authors have pointed out that the annealing temperature necessary for $L1_0$ phase formation in FePd nanoparticles is 100 K lower than that of the FePt nanoparticles.[9] The observed difference in ordering temperature between the FePd and FePt nanoparticles can be attributed to the difference in the melting temperatures of these alloys since it is well known that the diffusion constant is related to the inverse of the melting temperature of the concerned alloys. According to the binary alloy phase diagrams,[10] the melting temperatures of Fe, Co, Pt, and Pd decrease upon the addition of a small amount of Cu; in this sense, the additive Cu can increase the diffusivity of the constituent elements of FePt and FePd alloys. In fact, the ordering temperature was significantly decreased upon the addition of Cu in the case of an $L1_0$-FePt thin film.[11] In the case of an Fe–Pd–Cu system, a reduction of the atomic ordering temperature by 50 K in the FePdCu ternary alloy nanoparticles in comparison with that for the FePd alloy has been shown by our recent study.[12] However, structural features such as the particle size distribution, crystallographic orientation, and alloy composition of individual $L1_0$-FePdCu nanoparticles are yet to be investigated.

The present study aims at the structural characterization of oriented $L1_0$-FePdCu nanoparticles produced under the low annealing temperatures. The alloying of Cu into each FePd nanoparticle was confirmed by detailed transmission electron microscopy (TEM) analyses making use of electron diffraction and energy dispersive x-ray spectroscopy (EDS)

[a]Electronic mail: hirosi22@sanken.osaka-u.ac.jp

with nanoprobe electrons. The effect of Cu addition on the structure and the magnetic properties of the $L1_0$-FePd nanoparticles are discussed.

II. EXPERIMENTAL PROCEDURE

FePdCu nanoparticles were fabricated by the sequential deposition of Pd, Cu, and Fe by using an electron-beam evaporation apparatus on NaCl (001) single crystals cleaved in air. The base pressure before the deposition was approximately 1×10^{-6} Pa. Pure Fe (99.97%), Pd (99.95%), Cu (99.96%), and Al_2O_3 (99.99%) were used as evaporation sources. The specimen fabrication process consisted of three evaporation processes. First, the process took advantage of the growth of Cu on Pd "seed" nanoparticles, which were deposited prior to the Cu evaporation and epitaxially grown on the NaCl (001) substrates. Subsequently, Fe was deposited on the Cu–Pd nanoparticles. Pd, Cu, and Fe were deposited at a substrate temperature of 673 K. After the deposition of Fe, a thin amorphous film of Al_2O_3 was further deposited at a substrate temperature of about 523 K to prevent the oxidation of the particles and to stabilize them in a separated condition. A quartz thickness monitor attached to the chamber was used to estimate the average thickness of the deposited layer. The nominal average thicknesses of the Fe, Cu, and Pd were 1.8, 0.25, and 1.0 nm, respectively. The nominal thickness of the cover layer of Al_2O_3 was 10 nm. Besides the Fe–Pd–Cu ternary nanoparticles, we also fabricated Cu–Pd binary nanoparticles in order to confirm the Cu dissolution into Pd in the successive deposition process. The substrate temperature and growth rate of the Cu and Pd were the same as those for the FePdCu nanoparticles mentioned above, while the average deposited thicknesses of Cu and Pd were set to be 0.2 and 1 nm, respectively. The alloy composition of the FePdCu nanoparticles was controlled by changing the average thickness of each element. Postdeposition annealing was performed in a high vacuum furnace ($<2\times10^{-5}$ Pa) at 823 K for 3.6 ks on an alumina boat. The as-deposited and annealed films were removed from the NaCl substrates by immersing the substrates in distilled water. The films were then mounted on 400 mesh Cu and 200 mesh Mo grids for subsequent TEM observations, which were performed using 200 kV (JEM-2010) and 300 kV (JEM-3000F) electron microscopes. For the dark-field TEM observation, a LEO-922 200 kV TEM was used. The progress of the atomic ordering reaction was characterized by *in situ* TEM observations using a specimen heating stage with a Pt–Pt 13%Rh thermocouple. To calibrate the thermocouple, the atomic ordering temperatures of the as-deposited Fe/Pd and Fe/Pt nanoparticles observed by *in situ* annealing were compared to those of the particles obtained by *ex situ* annealing using an electric furnace; however, no apparent differences were observed between them. A compositional analysis was carried out by EDS on the annealed specimens mounted on the Mo grids. Their magnetic properties were measured using a superconducting quantum interference device (SQUID) magnetometer (MPMS-XL) in the temperature range between 10 and 300 K with a magnetic field of up to 50 kOe. The magnetic field was applied along both the film plane and the perpendicular direction.

III. RESULTS

A. Structure and morphology of Cu–Pd and FePdCu nanoparticles

Figure 1 shows the selected area electron diffraction (SAED) patterns and high-resolution TEM (HRTEM) images of the as-deposited Cu–Pd nanoparticles [Figs. 1(a) and 1(b)], as-deposited Fe/Cu–Pd nanoparticles [Figs. 1(c) and 1(d)], and $L1_0$-FePdCu nanoparticles after annealing at 823 K for 3.6 ks [Figs. 1(e) and 1(f)]. For the as-deposited Cu–Pd nanoparticles, a [001] zone axis diffraction pattern of fcc structure was observed in the SAED pattern shown in Fig. 1(a). A halo pattern from an a-Al_2O_3 thin film was also observed. The composition of each Cu–Pd nanoparticle analyzed by nanobeam EDS was almost the same as that of the mean composition of Pd–13 at. % Cu, which was within the solid solution compositional range according to the Cu–Pd binary phase diagram.[8] Crossed lattice fringes from {200} planes of Cu–Pd are visible in the HRTEM image shown in Fig. 1(b). We deduced the lattice constant of the Cu–Pd nanoparticles by analyzing the SAED patterns using polycrystalline Pd as a "standard" for the camera-length correction. The lattice parameters of the Cu–Pd nanoparticles as well as the values calculated from pure Pd and Cu on the basis of Vegard's law are shown in Table I. The observed lattice constant of the Cu–Pd nanoparticles was $a=0.386\pm0.001$ nm, which almost agrees with the reported value of $a=0.3854$ nm for the Pd–13 at. % Cu alloy obtained by Vegard's law. Hence, it is concluded that the successive deposition of Pd and Cu on the NaCl substrate maintained at 673 K resulted in the formation of Cu–Pd solid solution nanoparticles.

As shown in Fig. 1(c), reflections from bcc-Fe and Cu–Pd in addition to a weak halo pattern from the a-Al_2O_3 cover layer can be seen in the SAED pattern, whereas there are no superlattice reflections due to the $L1_0$ phase. A mutual fixed orientation relationship between Fe and Cu–Pd nanoparticles indicates the formation of the nanocomplex particles of Fe and Cu–Pd. The orientation relationship was as follows: $[100]_{Fe}\|[100]_{Cu-Pd}$, $(011)_{Fe}\|(010)_{Cu-Pd}$. The particle size distribution of Fe/Cu–Pd nanocomplex particles followed a log-normal-type distribution function with a mean particle size of 13.7 nm and standard deviation ln σ of 0.20. The particle size was defined as the arithmetical mean of the minor and major axes of the ellipse, and the total number of particles measured from the bright-field TEM images was 200. The areal density of the as-deposited Fe/Cu–Pd nanoparticles was 1.1×10^{11} cm^{-2}. The crossed lattice fringes from the {200} planes of Cu–Pd and {110} planes of Fe are visible in the HRTEM image shown in Fig. 1(d). The size of the dark contrast region is around 10 nm, which almost coincides with the average particle size of 9 nm of the Cu–Pd nanoparticles, indicating the formation of a core/shell structure[13] of Fe and Cu–Pd.

The specimen heating stage attached to the TEM was used for the *in situ* observation of the changes in the SAED

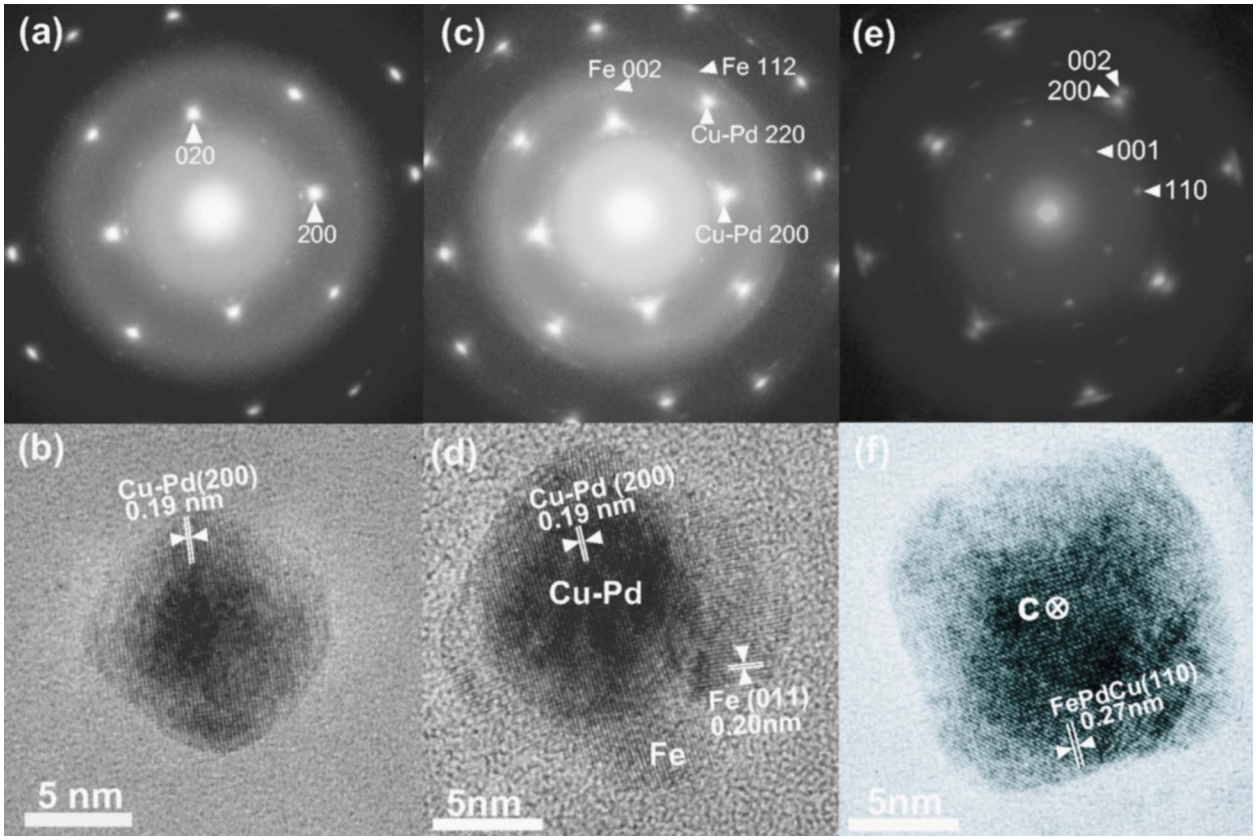

FIG. 1. SAED patterns and HRTEM images for Cu–Pd nanoparticles [(a) and (b)], as-deposited Fe/Cu–Pd nanoparticles [(c) and (d)], and $L1_0$-FePdCu nanoparticles after annealing at 823 K for 3.6 ks [(e) and (f)]. Crossed lattice fringes from the {200} plane of Cu–Pd and {110} plane of Fe are visible in an as-deposited Fe/Cu–Pd nanoparticle (d). {110} lattice fringes with a spacing of 0.27 nm of the tetragonal ordered structure can be seen in the image of an $L1_0$-FePdCu nanoparticle (f).

patterns during annealing. Weak 110 superlattice reflections from the $L1_0$-type ordered structure started to appear at 673 K. The intensity of the superlattice reflections increased with heating and became stronger above 723 K. These results indicate that the ordering temperature had reduced by 50 K due to the Cu addition, as compared with the case of the binary Fe–58 at. % Pd nanoparticles fabricated by the same technique.[14] Note that it has been reported that the atomic ordering temperature was substantially reduced to 573 K in the Fe–62 at. % Pt sputtered thin film due to the off-stoichiometric composition.[15] In the present study, however, such a large reduction of the atomic ordering temperature was not observed in the FePdCu nanoparticles with Pd concentrations between 38 and 57 at. %.

The superlattice reflections of the $L1_0$ structure can be clearly seen in Fig. 1(e), while other reflections are not observed from bcc-Fe or Cu–Pd, which indicates the formation of a single ternary $L1_0$-FePdCu phase after annealing at 823 K for 3.6 ks. We deduced the lattice constants of the $L1_0$-FePdCu nanoparticles after annealing at 823 K for 3.6 ks from the SAED patterns; they are summarized in Table I. The lattice parameters were $a=0.383\pm0.001$ nm and $c=0.355\pm0.002$ nm with an axial ratio of $c/a=0.928\pm0.006$. The obtained small axial ratio can be compared to that of $L1_0$-$FeCuPt_2$ ($c/a=0.923$) after annealing for a long time at 1473 K, indicating the high degree of order of the present specimen. The a-axis of the FePdCu nanoparticles was almost the same as that of the FePd nanoparticles [0.381±0.002 nm (Ref. 14)], while their c-axis was considerably smaller than that of FePd [$c=0.366\pm0.001$ nm (Ref. 14)], resulting in a small axial ratio. As mentioned above, the $L1_0$-ordered $FeCuPt_2$ also shows a smaller axial ratio than that of the FePt ($a=0.385\,25\pm0.000\,03$ nm, $c=0.371\,33\pm0.000\,05$ nm, and $c/a=0.9639$),[16] indicating that the additive Cu plays a role in reducing the axial ratio in $L1_0$-type ternary alloys. The average particle size of the $L1_0$-FePdCu nanoparticles was 14.3 nm with $\ln\sigma=0.16$. The particle areal number density covering the substrate was 1.1×10^{11} cm^{-2}. The nanoparticle size and areal density did not change even after annealing at 823 K for 3.6 ks, indicating that less coalescence growth occurred during annealing under these conditions. Therefore, it is considered that both alloying and the atomic ordering reactions proceeded within each nanoparticle. The strong central dark contrast observed

TABLE I. Lattice parameters of the Pd–Cu, $L1_0$-FePd, and $L1_0$-FePdCu alloy nanoparticles.

	a (nm)	c (nm)	c/a	Ref.
fcc-Pd–Cu	0.386±0.001 0.3854 (Vegard's law)			
$L1_0$-FePd	0.381±0.002	0.366±0.001	0.959±0.004	11
$L1_0$-FePdCu	0.383±0.001	0.355±0.002	0.928±0.006	

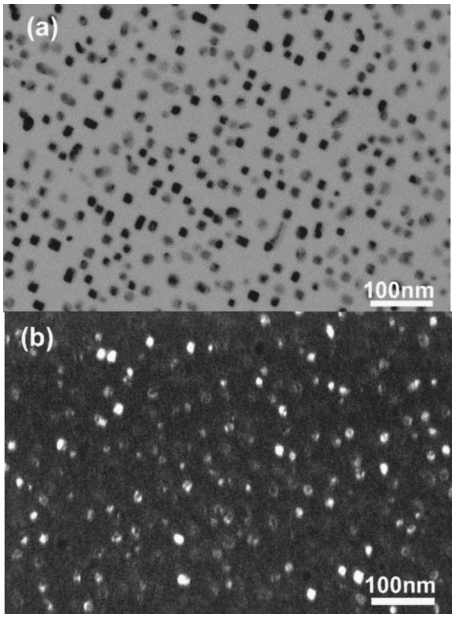

FIG. 2. Bright-field (a) and corresponding dark-field TEM images (b) for the $L1_0$-FePdCu nanoparticles after annealing at 823 K for 3.6 ks. A superlattice reflection of 110 was used for the dark-field TEM observation.

in the as-deposited nanoparticles extended rather homogeneously after annealing at 823 K for 3.6 ks, as shown in Fig. 1(f). The contrast change can be attributed to the promotion of the alloying and atomic ordering reactions in each nanoparticle by annealing. Most of the annealed nanoparticles are facetted with edges along $\{110\}_{FePdCu}$ due to the preferential c-axis orientation. Actually, the intensity of the 110 superlattice reflections was much stronger than that of the 001, indicating a preferential orientation of the crystallographic c-axis perpendicular to the film plane. In order to investigate the preferential orientation of the c-axis of the FePdCu nanoparticles, we performed a dark-field TEM observation of the above annealed specimen by using a 110 superlattice reflection. Figures 2(a) and 2(b) show a bright-field and the corresponding dark-field TEM images, respectively. A considerable number of nanoparticles were observed with a bright contrast in the dark-field TEM image. As a result, 74% of the FePdCu nanoparticles have their c-axis oriented perpendicular to the film plane, according to the areal number density of the bright contrasts. On the other hand, for binary FePd nanoparticles without Cu additives, the number of particles with their c-axis oriented perpendicular to the film plane was about 40%–50%, indicating that a small amount of Cu addition must be responsible for the presently observed high degree of preferential c-axis orientation along the film normal direction. In the next section, we focus on the characterization of the nanostructure of the $L1_0$-ordered FePdCu nanoparticles by using nanobeam EDS and nanobeam diffraction (NBD).

B. Particle size dependence of the alloy composition and axial ratio

The compositions of individual $L1_0$-FePdCu nanoparticles after annealing at 823 K for 3.6 ks were analyzed using nanobeam EDS to confirm the existence of Cu in each

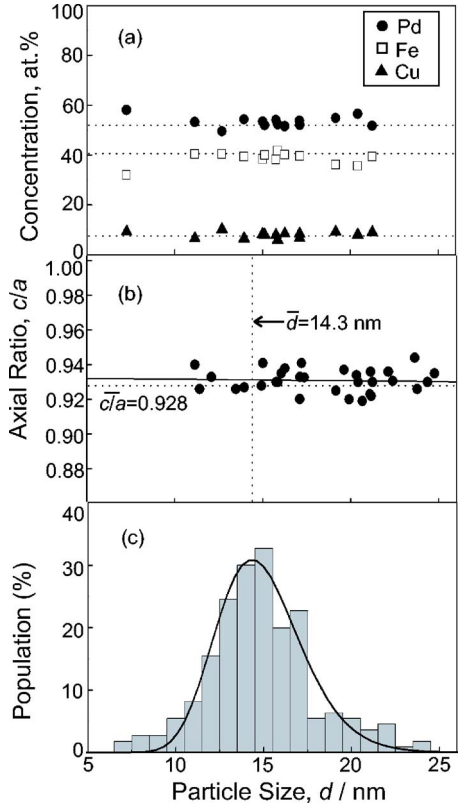

FIG. 3. Particle size dependence of the alloy composition (a) and the axial ratio c/a (b) determined by nano-EDS and NBD. A histogram of the particle size distribution of the $L1_0$-FePd nanoparticles after annealing at 823 K for 3.6 ks is also shown. The solid line indicates the fitting curve for the log-normal distribution function. The compositions of the individual nanoparticles were almost the same as the average composition in the entire particle size range. The axial ratios were in the range between 0.92 and 0.94.

nanoparticle. In these analyses, we used a condenser aperture with a diameter of 20 μm and a nanoprobe size of about 4 nm in full width at half maximum of the electron beam, which was smaller than the corresponding particle sizes. From the integrated intensity for the Fe-$K\alpha$ characteristic x ray, the statistical error was estimated to be about 4%. Figure 3(a) shows the particle size dependence of the alloy composition measured from individual $L1_0$-FePdCu nanoparticles. The broken lines indicate the average composition of $Fe_{41}Pd_{52}Cu_7$ measured from a wide area of the specimen film. The analyzed composition of each FePdCu nanoparticle was almost the same as that of the average over the wide region. The standard deviations of the alloy composition distribution for the Pd, Fe, and Cu contents are 2.5, 1, and 2 at. %, respectively; these values are quite small and comparable to the standard deviation of 3 at. % Pd for the binary Fe–58 at. % Pd nanoparticles.[17] The alloying of additive Cu into each $L1_0$ nanoparticle has been confirmed by the above analysis.

The magnetic properties of the $L1_0$-FePdCu nanoparticles depend on the degree of order of the $L1_0$ structure. The long-range order parameter is related to the axial ratio; therefore, in this study, we measured the axial ratio and its particle size dependence by analyzing the NBD patterns. Individual c/a ratios could be measured from the nanoparticles whose c-axis was oriented parallel to the film plane. The present

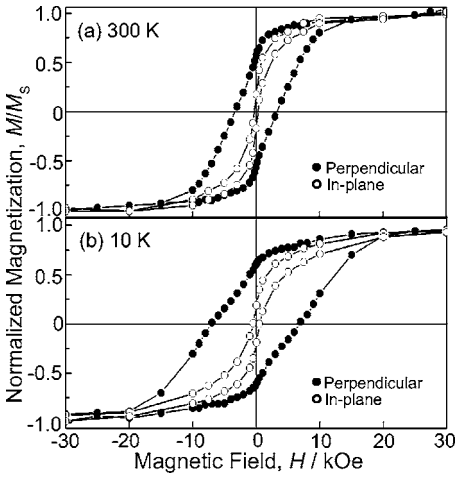

FIG. 4. Magnetization curves for the $L1_0$-FePdCu nanoparticles measured at 300 and 10 K after annealing at 823 K for 3.6 ks with the external magnetic field perpendicular (solid circles) and parallel (open circles) to the film plane.

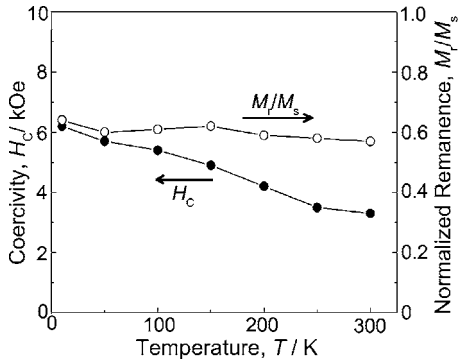

FIG. 5. Temperature dependence of the coercivity (solid circles) and normalized remanence (open circles) of the $L1_0$-FePdCu nanoparticles after annealing at 823 K for 3.6 ks.

specimen, however, has a larger population of FePdCu nanoparticles with their *c*-axis oriented perpendicular to the film plane. Within such an experimental limitation, we obtained the particle size dependence of c/a in a limited particle diameter range—between 10 and 25 nm—as shown in Fig. 3(b). The c/a dependence on particle size was almost parallel to the horizontal axis, indicating that the degree of order must be a constant value for FePdCu nanoparticles having particle size between 10 and 25 nm since no apparent particle size dependence was observed in the axial ratio. Actually, according to our previous study, a decrease in the order parameter with particle size reduction was observed for FePd nanoparticles with diameters smaller than 8 nm.[17] The particle size distribution shown in Fig. 3(c) indicates that FePdCu nanoparticles with diameters larger than 10 nm correspond to 92.6% of the population. In other words, about 92.6% of the FePdCu nanoparticles in the present specimen are considered to have a constant magnetocrystalline anisotropy energy, since the axial ratio is almost constant for these particles. It was concluded from the structural analyses that the magnetic properties of $L1_0$-FePdCu nanoparticles can be discussed under the condition of an almost fixed magnetocrystalline anisotropy constant regardless of the particle size distribution.

C. Magnetic properties of the $L1_0$-FePdCu nanoparticles

The magnetization curves of the $L1_0$-FePdCu nanoparticles measured at 10 and 300 K after annealing at 823 K for 3.6 ks are shown in Figs. 4(a) and 4(b), respectively. The magnetization curves measured perpendicular to the film plane showed a high coercivity of 3.6 kOe at 300 K. The annealing temperature necessary for obtaining a high coercivity decreased by 50 K as compared with the binary FePd nanoparticles.[14] In contrast, the magnetization curves measured along the in-plane direction showed considerably lower coercivities. A large difference in the normalized remanence was also observed between the perpendicular and in-plane magnetization curves. The normalized remanence of the FePdCu nanoparticles after annealing at 823 K was 0.61 for the perpendicular magnetization curve, while it was less than 0.14 for the in-plane one. The strong perpendicular magnetic anisotropy enhanced by a small amount of Cu addition can be attributed to the strong preferential perpendicular orientation of the crystallographic *c*-axis, as indicated by the dark-field TEM image shown in Fig. 2(b). The coercivity for the perpendicular direction increased as the measuring temperature decreased and reached 7.2 kOe at 10 K [Fig. 4(b)] due to a decrease in the thermal agitation of the magnetic moment as well as an increase in the magnetocrystalline anisotropy constant. Although Cu addition hindered the saturation magnetization and the magnetocrystalline anisotropy energy, the coercivity did not decrease drastically by the addition of a small amount of Cu. In comparison with our previous study on FePd nanoparticles, the FePdCu nanoparticles in the present study have relatively larger particle sizes, and as a result, a slight shrinkage of the magnetization curves near the remanence, which was clearly observed in the previous FePd nanoparticles,[14] was not apparent in the FePdCu nanoparticles in the present study. Actually, as mentioned above, the degree of order decreased when the particle diameter reduced below 8 nm in the case of binary FePd nanoparticles. The population of nanoparticles smaller than 8 nm was 6.5% in the previous FePd nanoparticles and 4.0% in the present FePdCu nanoparticles in this study. The relatively larger population of nanoparticles smaller than 8 nm is responsible for the previously observed shrinkage in the magnetization curve, since the alloy composition distribution from one particle to the next was found to be a small value around 2 at. % in standard deviation according to the compositional analyses by nanobeam EDS, as mentioned in Sec. III B. The temperature dependence of the coercivity and normalized remanence are shown in Fig. 5. These are obtained from the magnetization curves measured with the magnetic field applied perpendicular to the film plane at each temperature. There was a large monotonous increase in the coercivity as the temperature decreased. On the other hand, the remanence shows a small temperature dependence and remains at an almost constant value of 0.6. According to a recent computational study, the remanence is largely affected by both magnetostatic and exchange interactions among the particles.[18] However, in our FePdCu nanoparticles, both in-

terparticle magnetostatic and exchange interactions are negligible since the uniaxial magnetocrystalline anisotropy energy of the $L1_0$ phase is considered to be considerably higher than the interparticle magnetostatic interactions and also because the FePdCu nanoparticles are well isolated beyond the effective distance for the magnetic interaction by the a-Al_2O_3 thin film, as revealed by TEM observations. Hence, the observed small temperature dependence of the remanence indicates that, although the thermal fluctuation of the magnetization exists, its contribution is not so significant at temperatures below 300 K. For a system with considerable fluctuations, the remanence increases significantly as the temperature decreases.[19] Superparamagnetic behavior in smaller sized $L1_0$-FePd nanoparticles is now under investigation.

IV. DISCUSSION

From the results obtained in the previous section, the structural features of the present $L1_0$-FePdCu nanoparticles are summarized as follows: (1) isolated single crystal with a mean size of 14.3 nm with 1n σ=0.16; (2) homogeneous alloy composition; (3) almost homogeneous axial ratio for particle sizes larger than 10 nm, which correspond to 92.6% in terms of population; and (4) preferential c axis perpendicular orientation of about 74%. It has been reported that $L1_0$-FePt nanoparticles with diameters smaller than 20 nm act as single magnetic domain particles with a coherent rotation of magnetization.[20] As a consequence of these structural features, the magnetic interaction among the particles is negligible. Further, to some extent, the magnetization process can be simply discussed based on the concept of rotation magnetization of each nanoparticle against the magnetic anisotropy energy barrier under the thermal effect. It should be noted here that a correlation was observed between the crystallographic orientation of the FePdCu nanoparticles and the coercivity as well as the normalized remanence. According to the dark-field TEM observation, 74% of the nanoparticles have their c axis oriented perpendicular to the film plane and the remaining 26% have their c axis parallel to the film plane. There exist two types of orthogonal orientation of the c axis in the film plane: one parallel to the [100] of the NaCl substrate and the other parallel to the [010], based on the orientation relationships in the epitaxial growth. Note that no apparent difference or preferential orientation of the c axis was observed in the in-plane direction; therefore, the population of the nanoparticles with their c axis oriented parallel to [100] and [010] of the NaCl substrate are thought to be identical. Hence, the ratio of the nanoparticles with their c axis oriented perpendicular and in the in-plane ([100] or [010]) directions is calculated to be 74/13=5.7. On the other hand, the ratio of their perpendicular coercivity to their in-plane coercivity is about 3.6 kOe/0.6 kOe=7.0, which numerically agrees with the value of the c-axis orientation. In our previous study on $L1_0$-FePd nanoparticles, the coercivity ratio was determined to be 3.5 kOe/2.5 kOe=1.4, which agrees with the c-axis orientation value of 1.3–2. This was because the population of the FePd nanoparticles with their c axis oriented perpendicular to the film plane was 40%–50%, as seen from the dark-field TEM images. Therefore, it should be noted that for isolated single crystalline magnetic nanoparticles with relatively higher uniaxial magnetocrystalline anisotropy and insignificant interparticle magnetic interactions, the coercivity and remanence directly reflect the population of nanoparticles oriented along the magnetic easy axes.

V. CONCLUSION

An assembly of 14-nm-sized isolated $L1_0$-FePdCu nanoparticles has been fabricated by the successive deposition of Pd, Cu, and Fe on a NaCl (001) substrate cleaved in air, followed by postdeposition annealing. *In situ* TEM observations revealed that the atomic ordering reaction towards the $L1_0$ phase started at temperatures above 673 K. These particles were epitaxially grown on the substrate and were well isolated from each other. The isolation of each particle was kept even after annealing at 823 K. The alloy composition of each FePdCu nanoparticle was found to be almost independent of the particle size, based on EDS analyses using nanoprobe electrons. The alloying of additive Cu into individual FePd nanoparticles was confirmed experimentally in this study. The axial ratios of each nanoparticle remain constant for FePdCu nanoparticles with particle sizes between 10 and 25 nm. HRTEM observations revealed that these ternary alloy nanoparticles were $L1_0$-ordered structures with a preferential perpendicular orientation of the c-axis. Dark-field TEM observations revealed that the population of nanoparticles with their c-axis oriented normal to the film plane was 74%. The high coercivity of 3.6 kOe with strong perpendicular magnetic anisotropy was enhanced in the $L1_0$-FePdCu nanoparticles in this study. Magnetostatic and exchange interactions played an insignificant role in the present isolated FePdCu nanoparticles. The coercivity and remanence directly reflect the population of oriented nanoparticles for the isolated single crystalline FePdCu nanoparticles with relatively higher uniaxial magnetocrystalline anisotropy. In the present study, a strong preferential c-axis orientation and decrease in the ordering temperature has been achieved by the addition of a small amount of Cu into FePd nanoparticles.

ACKNOWLEDGMENTS

One of the authors (H.N.) wishes to express his gratitude to Dr. A. Hirata of ISIR, Osaka University for the LEO-922 TEM observations. This study was partially supported by the Center of Excellence (COE) program at ISIR, Osaka University, and the Grant-in-Aid for Scientific Research (S) (No. 16106008) from the Ministry of Education, Culture, Sports, Science, and Technology, Japan.

[1] R. H. Victora, J. Xue, and M. Patwari, IEEE Trans. Magn. **38**, 1886 (2002).
[2] D. J. Sellmyer, M. Yan, Y. Xu, and R. Skomski, IEEE Trans. Magn. **41**, 560 (2005).
[3] D. Weller and K. F. Doerner, Annu. Rev. Mater. Sci. **30**, 611 (2000).
[4] *Magnetic Properties of Fine Particles*, edited by J. L. Dormann and D. Fiorani (North-Holland, Amsterdam, 1992).
[5] J. L. Dormann, D. Fiorani, and E. Tronc, Adv. Chem. Phys. **98**, 283 (1997).
[6] For example, *Abstract of the Conference on $L1_0$ Ordered Intermetallic and*

Related Phases for Permanent Magnetic and Recording Applications, Copper Mountain, Co, 15–20 August 2004 (Engineering Conference International, Brooklyn, NY, 2004).
[7]C. P. Luo and D. J. Sellmyer, Appl. Phys. Lett. **75**, 3162 (1999).
[8]S. Sun, C. B. Murray, D. Weller, L. Folks, and A. Moser, Science **287**, 1989 (2000).
[9]K. Sato, B. Bian, and Y. Hirotsu, Jpn. J. Appl. Phys., Part 2 **39**, L1121 (2000).
[10]*Binary Alloy Phase Diagrams*, 2nd ed., edited by T. B. Massalski, H. Okamoto, P. R. Subramanian, and L. Kacprzak (ASM International, Materials Park, OH, 1990), pp. 1408 and 1450.
[11]T. Maeda, T. Kai, A. Kikitsu, T. Nagase, and J. Akiyama, Appl. Phys. Lett. **80**, 2147 (2002).
[12]H. Naganuma, K. Sato, and Y. Hirotsu, J. Appl. Phys. **99**, 08N706 (2006).
[13]B. Bian, Y. Hirotsu, K. Sato, and A. Makino, J. Electron Microsc. **48**, 753 (1999).
[14]K. Sato and Y. Hirotsu, J. Appl. Phys. **93**, 6291 (2003).
[15]T. Seki, T. Shima, K. Takahashi, Y. Takahashi, E. Matsubara, and K. Hono, Appl. Phys. Lett. **82**, 2461 (2003).
[16]JCPDS Card No. 43–1359.
[17]K. Sato, Y. Hirotsu, H. Mori, Z. Wang, and T. Hirayama, J. Appl. Phys. **98**, 024308 (2005).
[18]C. Verdes, B. Ruiz-Diaz, S. M. Thompson, R. W. Chantrell, and A. Stancu, Phys. Rev. B **65**, 174417 (2002).
[19]Y. Park, S. Adenwalla, G. P. Felcher, and S. D. Bader, Phys. Rev. B **52**, 12779 (1995).
[20]S. Okamoto, O. Kitakami, N. Kikuchi, T. Miyazaki, Y. Shimada, and Y. K. Takahashi, Phys. Rev. B **67**, 094422 (2003).